AGU100 ADVANCING EARTH AND SPACE SCIENCE

Global Biogeochemical Cycles

RESEARCH ARTICLE
10.1029/2017GB005840

Key Points:
- Active-layer tundra soils are high in soil mercury (Hg) concentrations despite the tundra's remote location
- Tundra soil Hg is derived from both recent and long-term atmospheric deposition that accumulated in deeper soils through many millennia
- Tundra Hg pools sizes are large (184 Gg), determined by depth of the active layer and mineral horizons, and form a large global pool of Hg

Supporting Information:
- Supporting Information S1

Correspondence to:
D. Obrist,
Daniel_Obrist@uml.edu

Citation:
Olson, C., Jiskra, M., Biester, H., Chow, J., & Obrist, D. (2018). Mercury in active-layer tundra soils of Alaska: Concentrations, pools, origins, and spatial distribution. *Global Biogeochemical Cycles*, *32*, 1058–1073. https://doi.org/10.1029/2017GB005840

Received 14 NOV 2017
Accepted 6 JUN 2018
Accepted article online 19 JUN 2018
Published online 20 JUL 2018

Mercury in Active-Layer Tundra Soils of Alaska: Concentrations, Pools, Origins, and Spatial Distribution

C. Olson[1], M. Jiskra[2], H. Biester[3], J. Chow[1], and D. Obrist[1,4]

[1]Desert Research Institute, Reno, NV, USA, [2]Geosciences Environment Toulouse, CNRS, Toulouse, France, [3]Environmental Geochemistry, Technische Universität Braunschweig, Braunschweig, Germany, [4]Department of Environmental, Earth and Atmospheric Sciences, University of Massachusetts, Lowell, MA, USA

Abstract Tundra soils serve as major sources of mercury (Hg) input to the Arctic Ocean via river runoff and coastal erosion; yet little information is available on tundra soil Hg concentrations, pool sizes, origins, and dynamics. We present a detailed investigation of Hg in the active layer (upper ~100 cm subject to seasonal thaw) of tundra soils across 11 sites in Alaska. Soil Hg concentrations in organic horizons (151 ± 7 μg/kg) were in the upper range of temperate soil organic horizons, and concentrations in mineral horizons (98 ± 6 μg/kg) were much higher than in temperate soils. Soil Hg concentrations declined from inland to coastal sites, in contrast to a hypothesized northward increase expected because of proximity to coastal atmospheric mercury depletion events. Principle component analyses and elemental ratios results show that exogenic sources dominated over geogenic sources—in A-horizons (66 ± 4%) and mineral B-horizons (51 ± 1%). ^{14}C age-dating suggested recent origins of Hg in surface soils but showed that mineral soils (more than 7,300 years old) must have accumulated atmospheric inputs across millennia leading to high soil concentrations and pools. We estimated a total Northern Hemisphere active-layer tundra soil Hg pool of 184 Gg (range of 136 to 274 Gg), suggesting a globally important Hg storage pool. Tundra soils are subject to seasonal thaw and freeze dynamics, thereby providing large inputs to rivers, lakes, and the Arctic Ocean. Understanding processes that mobilize Hg from tundra soils will be critical to understanding future Arctic wildlife and human Hg exposures.

1. Introduction

Upland soils act as buffers for Hg transfer between atmospheric deposition and runoff to streams and lakes (Lorey, 1999). Soils also serve as the main source of Hg to many lakes (Henning et al., 1989; Lindqvist et al., 1991), often exceeding direct atmospheric deposition. Turnover, dynamics, and mass balances of Hg in soils still have many uncertainties. For example, some studies indicate that as much as 25% of atmospheric Hg deposited to upland terrestrial basins reaches lakes (Mierle & Ingram, 1991; Swain et al., 1992), while others showed as little as 1% mobilization of atmospheric deposition from uplands to proximate lakes (Harris et al., 2007).

Only a few studies exist on Hg dynamics in Arctic tundra soils, despite their critical role as an Hg source to Arctic lakes, rivers, and the Arctic Ocean. The tundra biome accounts for roughly 6% of the Earth's surface (Bailey, 2014), and tundra soils are considered the dominant source of Hg to Arctic rivers and lakes (Fitzgerald et al., 2005; Klaminder et al., 2008; Rydberg et al., 2010). Fitzgerald et al. (2005) showed that upland tundra soils are the largest single source of Hg loading in lakes of northern Alaska. Seasonal freshwater discharge from snowmelt and soil thaw releases large amounts of sediment as well as dissolved and particulate organic carbon (DOC and total organic carbon) to major Arctic rivers that drain into the Arctic Ocean (Dittmar & Kattner, 2003). Along with sediment and organic carbon transport, large amounts of Hg are mobilized from upland soils to the Arctic Ocean (Emmerton et al., 2013; Leitch et al., 2007; Schuster et al., 2011), including from the Mackenzie (2.3–4.2 Mg/year; Emmerton et al., 2013) and Yukon rivers (4.4 Mg/year; Schuster et al., 2011). These Arctic rivers have 3 to 32 times larger Hg yields than reported from other major Northern Hemisphere (NH) river basins (0.4 to 4.4 Mg/year; Schuster et al., 2011). Recent model simulations estimated a range of annual fluxes between 46 and 95 Mg Hg/year (Dastoor & Durnford, 2014; Fisher et al., 2012; Zhang et al., 2015) from Arctic rivers to the Arctic Ocean, plus 15 Mg Hg/year from coastal erosion (Fisher et al., 2012). This annual flux exceeds direct atmospheric Hg deposition to the ocean (Fisher et al., 2012). The dominance of upland runoff and erosion sources to the Arctic Ocean contrasts with other ocean basins where direct atmospheric Hg deposition generally dominates (Soerensen et al., 2016).

The Arctic in modern times has experienced increased atmospheric Hg inputs and increased methylmercury production compared to preindustrialization (Hammerschmidt et al., 2006). Arctic sediments show a 3-to-5 times increase in atmospheric deposition loads since the Industrial Revolution (Fitzgerald et al., 2005), similar to those found in temperate zones (Drevnick et al., 2016; Schuster et al., 2002). This modern increase in Arctic Hg deposition has led to increased biological exposure as confirmed, for example, by Arctic animal tissue collections showing a 14-fold increase in Greenlandic polar bear hair Hg concentrations since 1300 CE (Dietz et al., 2006) and a fourfold increase of Hg in teeth of Beluga Whales since 1650 CE (Outridge et al., 2002). Elevated mercury concentrations in the Arctic also pose a threat to indigenous groups that rely on Arctic wildlife for food (AMAP, 2011). Higher intake of methylmercury has led to tenfold higher blood mercury concentrations in the Inuit population of Nunavut (Arctic Canada) than those living in southern Quebec (Laliberté et al., 1992) and a possible risk of fetal toxicity among more than 90% of child-bearing women (Ayotte et al., 2001). Additionally, one in four children from Nunavut exceeded the World Health Organization reference value for hair Hg concentration because of higher than acceptable levels of methylmercury intake (Tian et al., 2011).

The objectives of this study were to (1) assess the spatial (both horizontal and vertical) distribution of upper soil Hg concentrations in the active layer of tundra soils (i.e., soils that are subject to seasonal thaw); (2) assess the degree to which active-layer tundra soil Hg is derived from atmospheric versus geogenic sources by means of comparisons to crustal elements and stable isotope analysis; (3) characterize associations of soil Hg with soil organic carbon (OC), pedogenetic characteristics, soil age, and major and trace elements to assess factors that determine Hg accumulation in tundra soils; and (4) use these data along with further published data on Arctic tundra soil Hg to extrapolate active-layer tundra soil Hg pools across the tundra (upper 1 m) to assess pool sizes located in the active-layer zone. We compared results to a recent study by Schuster et al. (2018), who measured Hg concentrations across 13 permafrost cores to depths of 166 cm, and reported Hg concentrations ranging from 17 to 207 μg/kg (mean of 64 μg/kg) in the permafrost zone and concentrations of 50 to 100 μg/kg in the active-layer zones. They estimated that NH Hg pool size may contain an enormous amount of Hg (1,656 Gg) in permafrost soils, roughly half of which was estimated to be located in the continually frozen permafrost zone. Their study, however, did not elucidate the dynamics of Hg in active-layer Hg zones and horizons, or origins of Hg in different layers. Our findings should help to understand how much Hg is accumulating in Arctic tundra soils, characterize sources in soil horizons, determine physical and chemical factors that are related to Hg accumulation, and help constrain the fate of Hg contained in these highly dynamic, seasonally thawing, active-layer soil horizons.

2. Methods

2.1. Study Sites

The main study site was located at Toolik Field station in northern Alaska (68°38′N, 149°36′W; Figure 1). Toolik Field station is at an elevation of 720 m above sea level with a mean annual precipitation of 312 mm and a mean annual air temperature of −8 °C (Lee, 2015). The site is dominated by an acidic tussock tundra (Shaver & Chapin, 1991) with dominant species including *Cetraria kamczatica Savicz* (white lichen), *Masonhalea richardsonii* (*Hook.*) *Karnefelt* (brown lichen), *Hylocomium splendens* (*Hedw.*) *Schimp.* (feather moss), *Carex aquatilis Wahlenb.* (tussock grass), and *Betula nana* L. (dwarf birch). This site is characterized as moist-to-wet tundra with Typic Aquiturbel soils.

Seven additional sites were chosen along a 200 km stretch of the Dalton Highway between Toolik Field station and Deadhorse near the Arctic Ocean (Figure 1b and Table S1). These sites were co-located with previous soil surveys by the U.S. Department of Agriculture Natural Resource Conservation Service (Michaelson et al., 2013). Four of the sites were located in moist acidic tundra, and three of the sites were located in moist nonacidic tundra (Borden et al., 2010). Moist acidic tundra vegetation is characterized by tussock grass, ericaceous shrubs, and sphagnum moss (Borden et al., 2010). Moist nonacidic tundra vegetation is characterized by sedges, prostrate shrubs, and peat moss (Borden et al., 2010). Moist nonacidic soils are more neutral to alkaline as a result of recent deposits of calcareous loess from the banks of the Sagavanirktok River (Borden et al., 2010). Four of the sites were located in the Sagwon Hills region, part of the northern foothills of the Brooks Range in northern Alaska. This area is characterized by rolling hills with gentle slopes (maximum 20%) and has a mean annual precipitation of 140 to 270 mm (Ping & Moore, 1993) and a mean annual air temperature of −6 to −4 °C (Zhang et al., 1996).

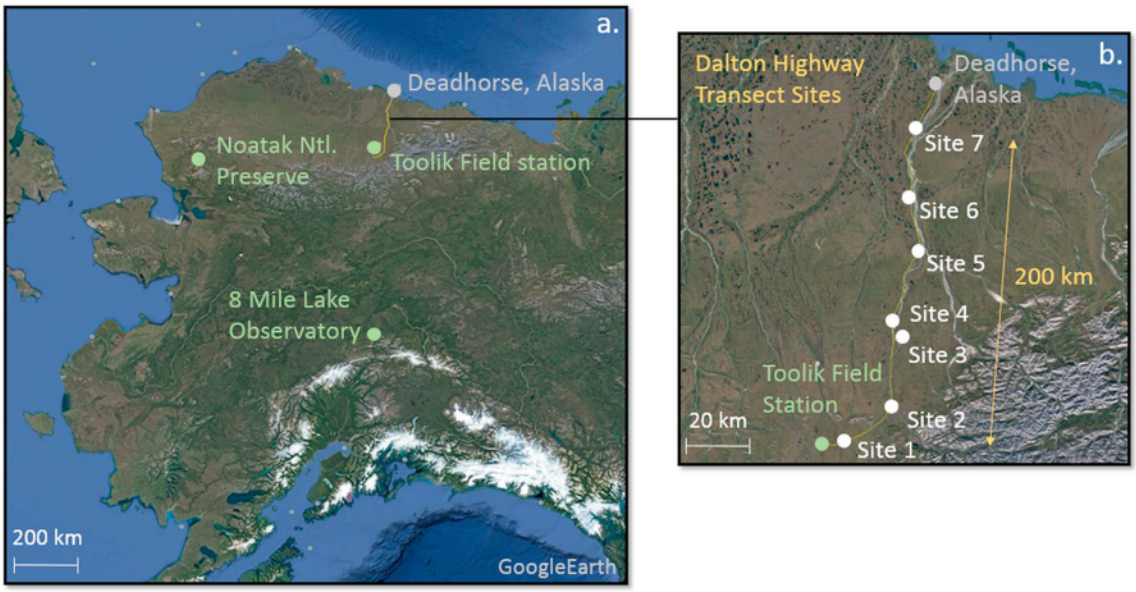

Figure 1. Research sites used in this study. (a) The main research site was characterized as Tussock tundra located at Toolik Field Station in northern Alaska, with additional sites located in NW Alaska at the Noatak National Preserve and near Denali National Park in interior Alaska. (b) Seven sites were chosen along a 200 km transect following the Dalton Highway.

Another study site was at the Eight Mile Lake watershed near the northeast corner of Denali National Park and Preserve in central Alaska (63°52′59″N, 149°13′32″W). Eight Mile Lake is at an elevation of 700 m on a relatively well-drained, gentle, northeast facing slope with a mean annual air temperature of −2.8 °C (Natali et al., 2014). The vegetation at this site is characterized by moist acidic tussock tundra and is underlain by continuous permafrost within the watershed despite being located in a zone of discontinuous permafrost (Webb et al., 2016). Dominant species at this site included white lichen, brown lichen, feather moss, tussock grass, and dwarf birch. Soils here are classified as Gelisols with an organic horizon 45–65 cm thick above a cryoturbated mineral soil that is a mixture of glacial till and windblown loess (Lee et al., 2010).

A further study site was located in the Noatak National Preserve in northwestern Alaska. At this location, the following three subsites were sampled and included: Asik (67°28′31″N, 162°14′0″W), ANFT4 north facing (67°31′21″N, 162°3′48″W), and ANFT4 south facing tundra (67°31′26.04″N, 162° 3′ 33.696″W). The soils were characterized as Orthels under the Gelisol Order and were relatively ice-poor with minimal evidence of cryoturbation. Dominant vegetation species at the Asik site included *Picea glauca* (Moench) Voss (white spruce) with extensive feather moss cover. Dominant vegetation species at the ANFT4 north facing site included upland tussock tundra vegetation above the treeline with extensive peat moss cover, *Vaccinium uliginosium* L. bog (blueberry), and *Vaccinium vitaus-idaea* L. lingonberry (cranberry). The ANFT4 south facing site contained upland tussock tundra vegetation and extensive peat moss cover with blueberry and cranberry. Mean annual temperature at an elevation of 405 m was −2.9 °C, and the precipitation was roughly 250 mm based on snow depth sensor data (Western Regional Climate Center, 2005).

2.2. Sample Collection

We collected soil samples to the bottom of the unfrozen active layer using clean latex gloves and stainless steel tools washed with deionized water. Additionally, we collected bulk vegetation samples from the surface of the excavated soil pits. All samples were double-bagged in plastic zip-lock bags and stored on ice until transport to the laboratory where they were kept frozen at −20 °C until analysis. Soil pits were sampled in late July and early August of 2014 and 2015, coinciding approximately with the peak thawing depth of the active layer (maximum depth of 90 cm). Soil pits were vertically sampled by soil horizons from the surface to the permafrost zone or to the underlying bedrock. Organic soil horizons were determined visually according to the following standard protocols: Oi, fresh undecomposed surface litter; Oe, partially decomposed litter; and Oa, fully organic humus layer characterized by decomposition, whereby plant origin is no longer recognizable. Mineral soil A-horizons were determined by their darker gray color with high organic matter (OM)

content, and B-horizons were characterized by their lighter brown or gray color. The horizon separation between O-, A-, and B-horizons in the field based on color and soil characterization was confirmed by OM analysis in the laboratory (generally O: ≥20% OM and A: ≥10% OM). Buried organic horizons were present in some vertical profiles because of cryoturbation and were recognized by darker colored soil horizons buried within mineral horizons. We collected material from various walls of the pits per horizon and pooled samples into one composite sample per horizon for horizons ≤20 cm. For horizons >20 cm, two pooled samples were taken per horizon at upper and lower locations of the respective soil horizon. Bulk density in organic and mineral soil horizons was measured using a vertical ring sampler (Model 0200 Soil Core Sampler, Soilmoisture Equipment Corp., CA, USA) with a known volume that allows for uncompacted extraction of intact soil cores. Measured bulk density measurements were within the range of other Arctic tundra soil studies (Givelet et al., 2004). Soil pH was determined using a field soil pH testing kit during soil sampling and repeated with laboratory measurements (Metrohm, Zofingen, Switzerland) during sample processing.

Soil solution and water samples were collected from Toolik Field Station using soil lysimeters, at the bottom of excavated soil pits, and in nearby streams and rivers. We collected water samples using clean latex gloves into 50 ml Falcon Polypropylene Tubes (Corning, Corning, New York, USA) for determination of dissolved Hg and DOC analyses. Each Falcon tube was rinsed three times, and tubes were filled to the top leaving little to no air. Immediately after collection, water samples were taken to the Toolik Field Station wet laboratory and filtered into new 50 ml Falcon Polypropylene Tubes using sterile gloves and Acrodisc® syringe filters (Pall Corporation, New York, USA) with 0.45 μm Supor® membrane. Filtered samples were acidified by 5% vol/vol ultrapure grade HNO_3. Samples were taken in duplicates, and field blanks were analyzed for every 10 samples taken.

2.3. Sample Preparation and Analytical Methods

Soil and vegetation samples were oven-dried at 65 °C (Lindberg Blue M Premium 3055, Thermo Fisher Scientific, Waltham, Massachusetts, USA), a method that has been shown to not lead to loss of Hg from soils or vegetation (Hojdova et al., 2015; Yang et al., 2017). Samples were then hand ground using a ceramic mortar and pestle followed by sieving using a 2-mm diameter stainless steel sieve (FieldMaster, Science First, Florida, USA). Vegetation and organic horizon samples were ground using a stainless steel coffee mill. A portion of the oven-dried soil samples was milled using a tungsten-carbide mill (Model 8510 Shatterbox, SPEX SamplePrep, Metuchen, New Jersey, USA) for analysis of Hg, carbon, nitrogen, and other trace elements.

Sample Hg concentrations were measured using a total Hg analyzer (Model Nippon MA-2000, AGS Scientific Inc., Texas, USA) in accordance with U.S. Environmental Protection Agency (EPA) Method 7473 (EPA-U, 1998a). Calibration was based on standard solutions (100 and 10 μg/L) prepared according to EPA Method 1631 (EPA-U, 2002). National Institute of Standards and Technology (NIST) solid standard reference materials (# 1575: Pine leaves: 39.9 μg Hg/kg and # 1515: Apple Leaves: 44.4 μg Hg/kg) were measured at the beginning of each analytical run with measurement repeated after every four samples. When analysis of NIST standards deviated more than 5% from their values, we recalibrated the analyzer and re-ran all samples after the last acceptable NIST standard testing. All samples were analyzed in duplicate and averaged. A total of 120 soil samples were analyzed for this study. Five samples representing different soil horizons collected from Toolik Field station were sent to Eurofins Frontier Global Sciences (Seattle, WA) for analysis of monomethyl-Hg using a Tekran Series 2700 Automated Methyl Mercury Analyzer (Tekran Instruments Corporation, Toronto, Canada) following EPA method 1630 (EPA-U, 1998b).

Dried and milled samples were prepared for X-ray fluorescence (XRF) analysis (Model Epsilon 5 Energy Dispersive X-Ray Spectometer, PANalytical, Alemo, Netherlands) using a resuspension technique (Chow et al., 1994) to load bulk soil samples onto Teflon® filters, following EPA method IO 3.3 for filter analysis (U.S. EPA, 1999). This XRF analysis only measured total element concentrations and not speciation. Vegetation and soil total carbon (TC) and total nitrogen were analyzed using a LECO dry combustion procedure (LECO, St. Joseph, MI) at the Soil Forage and Water Analysis Laboratory of Oklahoma State University. Oklahoma State University calculated OM content based on reported TC concentrations using the Van Bemmelen factor of 1.724 (Ball, 1964). Eight mineral samples from Pits 1 to 4 were analyzed for inorganic carbonate (% mass) by the group of Professor R. Kretzschmar in the soil chemistry analytical laboratory at the Federal Institute of Technology (ETH) in Zürich, Switzerland. Carbonates were analyzed using a gravimetric

method: samples were acidified with 10% H_2SO_4 and weighed before and after to measure the loss of CO_2 adsorption in porous NaOH within a column. Soil pH was determined using a 1:1 ratio of organic and mineral soil to 0.1 M $CaC0_3$ solution with end-to-end shaking for 30 min, and pH was measured in the laboratory using a pH/ion analyzer (Model 827, Metrohm AG, Herisau, Switzerland). ^{14}C age dating was performed for three soil samples (Vegetation, Oe/Oa, and B Horizon from Pit 1) by the University of Arizona Accelerator Mass Spectrometry Laboratory using a Pelletron Accelerator Mass Spectrometer (3 MeV, National Electrostatics Corporation, WI, USA). Total Hg in solution samples was analyzed using a Tekran 2600 Hg Water Analyzer (Tekran Inc., Toronto, Canada) following U.S. EPA SM 1631, revision E for total mercury in water (EPA-U, 2002). The day before analysis, bromine chloride (BrCl) solution (10% vol/vol) was added to the samples to oxidize the solution Hg, and 30 min before analysis, excess BrCl was neutralized with prepurified hydroxylamine hydrochloride. During analysis, oxidized Hg is reduced to elemental Hg by automatic mixing with stannous chloride ($SnCl_2$) in a phase separator. Elemental Hg is then loaded onto two sequential gold traps by an argon carrier gas. The loaded Hg is released through thermal desorption and detected using atomic fluorescence spectrometry. The Tekran model 2600 was calibrated using a NIST SRM-3133 Hg standard concentrations diluted to 0, 0.5, 1.0, 5.0, 10.0, 25.0, and 50.0 ng/L Hg. System accuracy was checked using reagent blanks and ongoing precision recovery injections of 5 ng/L throughout each run.

2.4. Data Analysis, Enrichment Factors, and Principal Component Analyses

Variance shown in figures and tables represent standard errors. We used linear regression analyses to quantify relationships between dependent (Hg) and independent variables including soil horizon, pH, total nitrogen, and TC using Stata 12 software (StataCorp, 2011). Active-layer mercury pool sizes (in g/ha) for each soil pit were estimated by first calculating the mass of Hg stored in each soil horizon by multiplication of soil Hg concentrations with soil bulk density measurements and the respective soil-depth horizon. We then summed these horizon Hg masses together to estimate storage of Hg mass for each pit (in g/ha).

To determine potential origin of Hg, we performed detailed geochemical analyses of soil samples including XRF multielement characterization and quantified associations of Hg to other soil elements. In a first step, contributions of exogenic and lithogenic Hg were estimated using reference concentrations of geogenic elements that are not considered to be influenced by atmospheric sources. These calculations were based on methods used in Guedron et al. (2006) and Peña-Rodríguez et al. (2012). Guedron et al. (2006) estimated a theoretical "lithospheric" Hg concentration from weathering for each depth of the soil profile as

$$[\mathrm{Hg}]_{\mathrm{lithogenic}} = k_{p*}\frac{[\mathrm{Hg}]_p}{k_s} \quad (1)$$

where k is the reference element, the subscript s refers to soil material, and the subscript p refers to parent reference material. $[Hg]_p$ is the bedrock Hg concentration. For k_p, we used mean concentrations of Al, Ti, Fe, Zn, and Zr measured by XRF analysis from the lowest B horizon present at Toolik Field station, which are generally considered conservative, but may be enriched or depleted in B horizons due to pedogenetic processes. The Hg excess of measured samples compared to the lithospheric Hg concentrations was attributed to exogenic sources and calculated as

$$[\mathrm{Hg}]_{\mathrm{exogenic}} = [\mathrm{Hg}]_s - [\mathrm{Hg}]_{\mathrm{lithogenic}} \quad (2)$$

where $[Hg]_s$ refers to the measured Hg concentration of the respective soil material.

Finally, we performed a rank-based principal component analysis (PCA) using R packages "ade4" (Dray & Dufour, 2007) and "rgr" (Garrett, 2013) to assess relationships between Hg and other soil elements to determine and support source origins of Hg. The data were converted to the same units before running the R packages. PCAs were performed for select trace metals of Pits 1 to 8 along with soil Hg concentration and TC.

2.5. Arctic Hg Pool Size Calculations

We combined data of soil Hg, C, and Hg:C ratios from our study with 14 other Arctic studies (see the supporting information) for a total of 478 data points on active-layer tundra soil Hg concentrations. Using this data set, we estimated active-layer tundra Hg pool sizes for Arctic soils separated into upper (0–30 cm depth;

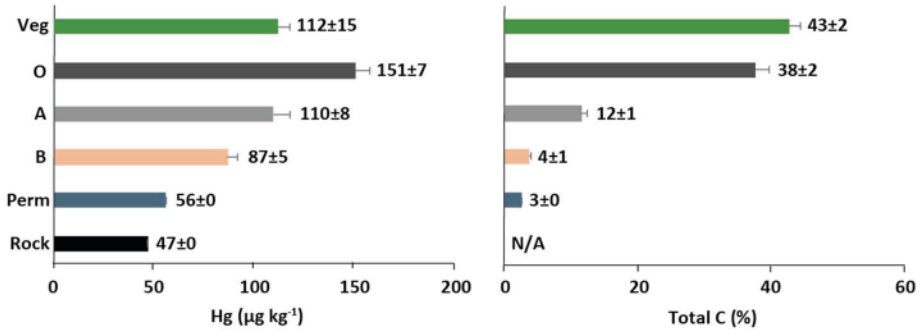

Figure 2. Mean Hg concentrations and total carbon for eight soil pits from Toolik Field station. Mean Hg concentrations (in μg/kg) in all soil pit layers, permafrost, and bedrock samples at the Toolik Field Station, and respective total carbon (in % mass) of samples.

assumed organic soils, TC content >19%) and deeper soils (30–100 cm; assumed mineral soils, TC content of 1–19%). Since most studies do not report soil bulk densities, we found that the best method for scaling up Hg concentrations to a pool size for the Arctic was by using Hg:C ratios from the data set and Arctic soil carbon inventories. We used Hugelius et al. (2014) global carbon estimates for permafrost soils of 217 Gg for the 0–30 cm depth and 255 Gg for the 30–100 cm depth and multiplied these by Hg:C ratios for both organic (0–30 cm) and mineral soils (30–100 cm). Based on summary statistics of Hg:C ratios, we estimated median and percentile ranges (37.5 to 67.5%) of Hg pool sizes for active-layer soils of the Arctic tundra. For comparison, we also collected published data on boreal soil Hg, C, and Hg:C ratios to estimate pool sizes for the global boreal zone, with a total of 479 available data points from the literature.

3. Results and Discussion

3.1. Hg Concentrations in Tundra Soils at Toolik Field Station

We first present results of eight soil pits from Toolik Field station—from the surface to the frozen underground or bedrock representing the thawed-layer (~active-layer) depth that we encountered in August (Figure S1). Of the eight vertical tundra soil profiles (all characterized as Gelisols), four pits (Pits 1, 2, 3, and 4) showed relatively shallow organic layers (<20 cm) and a high representation of mineral soil horizons, while four profiles (Pits 5, 6, 7, and 8) showed deeper organic horizons (>20 cm). Soil pH ranged from 3.7 to 7.5, with the lowest pH in surface organic and upper mineral soil (A-horizons) consistent with acidity inputs from plant exudates and decomposing plant OM. Analysis of inorganic carbonates in a subsection of samples (eight samples) in mineral soil horizons showed concentrations below detection limits (<0.01% C) to a maximum of only 1.9%. We concluded that inorganic carbonates did not contribute significantly to observed total C content and hence refer to results of total C analysis as OC. OC concentrations had a mean of 38 ± 1.7% in organic horizons, 10 ± 0.8% in A-horizons, and 2 ± 0.2% in B-horizons (Figure S1). OC strongly declined from surface organic layers to mineral soil layers because of plant-derived OC inputs from the surface as observed in other soils (Larcher, 1995).

Hg concentrations in the eight soil pits at Toolik Field station ranged from 56 to 226 μg/kg, showing large variability in concentrations (over fourfold). Summarizing Hg concentrations by pedogenic soil horizons showed the following depth and horizon patterns (Figure 2): Hg concentrations were highest in organic layers, ranging from 101 to 226 μg/kg with a mean Hg concentration of 151 ± 7 μg/kg. Hg concentrations in A-horizons were second highest and ranged from 79 to 149 with a mean of 108 ± 10 μg/kg. B-horizon Hg concentrations ranged from 56 to 102 μg/kg with a mean of 87 ± 5 μg/kg. Finally, lowest soil Hg concentrations were measured in the frozen horizon at the bottom of the pits (transient permafrost layers) with a mean of 56 ± 2 μg/kg. Rock Hg concentrations from samples obtained from the pits were 16 to 54% lower than those found in B-horizon Hg concentrations and had a mean of 47 ± 1 μg/kg.

Hg concentrations in surface organic horizons (organic horizons at Toolik Field station) with a mean of 151 ± 7 μg/kg were hence comparable or higher compared to organic horizon Hg concentrations generally reported from temperate sites (means of 102 to 140 μg/kg; e.g., 140 μg/kg, Grigal, 2003; and 102 μg/kg, Obrist et al., 2011). A- and B-horizon Hg concentrations (110 and 87 μg/kg), however, were considerably

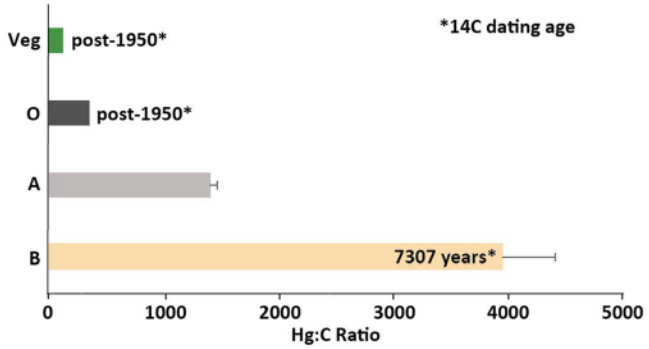

Figure 3. Hg to C ratios in Toolik Field station soil and vegetation samples. Hg to C ratios in vegetation and soil samples from the Toolik Field station with respective ^{14}C carbon dating age from selected representative samples (Pit 1 Oe/Oa, A, and B).

higher compared to levels reported in mineral soils across temperate locations (~34 μg/kg, Smith & Geological Survey, 2013; 24 μg/kg, Obrist et al., 2016; and 20 to 50 μg/kg; Amos et al., 2015). These high mineral soil Hg concentrations at a remote site such as Toolik field station, distant from many known Hg emission sources (Jaeglé, 2010), were unexpected (see discussion below), raising questions as to the origins of Hg in these tundra soils. Obrist et al. (2017) recently presented a comprehensive Hg-deposition mass balance study at this site showing that approximately 70% of Hg deposition was derived from gaseous elemental Hg deposition (Hg^0), with the remainder from deposition of oxidized Hg (Hg^{II}) by precipitation and atmospheric mercury depletion events (AMDEs). Deposition of Hg^0 occurred throughout the year and was enhanced in summer through uptake by vegetation, suggesting that the dominant source at this site was from deposition of Hg from a global atmospheric background pool, rather than specific regional or local sources. What is peculiar at this site was that almost no Hg re-emission was observed by Obrist et al. (2017), in contrast to periods of such Hg^0 volatilization losses back to the atmosphere at temperate sites (Smith-Downey et al., 2010). This dominance of atmospheric Hg^0 as a source in the tundra was confirmed by stable isotope data (Obrist et al., 2017) that showed that atmospheric Hg^0 accounted for 90% in vegetation, 73% in organic horizons, and 25% to 55% in mineral horizons. The deposition of global background Hg sources, along with a lack of re-emission, may be primary reasons for the high soil Hg concentrations and mass (see below) measured in these remote northern soils.

Particularly high Hg concentrations observed in lower soil layers may be linked to cryoturbation processes that lead to vertical downward mixing of surface layers into the lower soil profile (Ping et al., 1998). In addition, increased vertical transfer of Hg may occur during soil thawing and snowmelt that may facilitate transport of Hg to deeper soils, similar to vertical transport that has been reported for DOC during spring and summer (Klaminder et al., 2009). One of the few studies showing similarly high Hg concentrations in subsoils was from temperate podzols in which high mineral Hg concentrations were attributed to transport of complexed metals by DOC (Schwesig & Matzner, 2001). In addition, saturated conditions during part of the year, as well as annual snowmelt processes, may increase vertical translocation of Hg in Arctic soils, although further studies are needed to confirm this.

A question regarding sources of Hg in tundra soils is the deposition timeline. We performed radiocarbon (^{14}C) analyses of three samples (Figure 3) with results showing that upper soils (i.e., organic horizons) are young with a "postbomb" signature (i.e., post 1950s) suggesting recent formation of surface horizons (note, however, that ^{14}C age only reports the mean age so that this horizon may contain younger or older C as well). Our results suggest that Hg in organic surface soil was recently deposited and likely includes modern anthropogenic Hg emissions. ^{14}C data show that deeper, mineral-soil layers are much older, with a ^{14}C age of more than 7,300 years in the lower mineral B-horizon. This layer also shows the highest Hg:OC ratios (i.e., Hg concentrations standardized per unit OC; Obrist et al., 2011) of all soil layers. We attribute the dominant source of Hg in the mineral soil layers, and their respective high Hg concentrations and Hg:OC ratios, to old soil age indicating long-term input of atmospheric Hg sorbed in soils. Such legacy Hg accumulation has also been associated with a buildup of soil Hg pools in temperate soils (Obrist et al., 2011, 2016, 2017; Schwesig et al., 1999). To support this notion, we provide coarse mass balance calculations using estimated Hg mass in soils in section 3.4, showing that long-term atmospheric deposition of Hg is required to account for observed Hg pools in tundra soils.

Based on analysis of a small subset of five samples, we found that concentrations of monomethyl-Hg were 0.5 and 3.4 μg/kg in organic horizons and 0.1 and 1.0 μg/kg in B-horizons. One sample from the permafrost zone had a concentration below the detection limit (0.1 μg/kg). On average, MeHg accounted for 1% of total Hg (THg), with a maximum of 3% in the B-horizon. The percentage of MeHg to total Hg was relatively high in these samples; for example, the mean percentage of MeHg of THg at some temperate sites was only 0.2% to 0.6% (0.2% in Obrist, 2012; 0.6% in Grigal, 2003; 0.3% in Selvendiran et al., 2008; and 0.4% in Kronberg, Jiskra, et al., 2016). Although more samples are needed to confirm these results, it is possible that

saturated, anoxic conditions that promote MeHg formation in soils and sediments (Grigal, 2003; MacMillan et al., 2015) may be associated with higher MeHg levels in tundra soils.

3.2. Hg and Other Trace Elements in Tundra Soils at Toolik Field Station

As discussed above, stable Hg isotope analysis data suggest that the dominant source of Hg in the Arctic tundra (plants, litter, and soils) is derived from atmospheric Hg(0) deposition (Obrist et al., 2017). We used geochemical calculations in soils as an additional method to estimate contributions of exogenic Hg (i.e., from atmospheric deposition) versus lithogenic sources using reference concentrations of Al, Ti, Fe, Zn, and Zr measured in the lowest B-horizons and in rocks, following the methods described in Guedron et al. (2006) and Peña-Rodríguez et al. (2012). Note that this method may be compromised by the fact that parent material at this site consists of loess and glacial till so that soils may not necessarily be directly derived from the rocks collected in the soil pits at the site. Still, calculations support that exogenic Hg was the dominant source of Hg in soils, accounting for 66 ± 4% in A-horizons and 51 ± 1% in B-horizons. Hence, our calculations suggest similar proportions of exogenic atmospheric Hg contributions as measured by stable Hg isotope analyses, bedrock Hg concentrations, and mixing model analyses (Obrist et al., 2017) that showed 80% of Hg derived from exogenic sources in A mineral horizons and 61% in B-horizons. Obrist et al. (2017) further concluded that Hg in organic horizons was fully derived from atmospheric Hg deposition.

The levels of exogenic contributions in tundra soils hence are similar to those elswhere (Guedron et al., 2006; Peña-Rodríguez et al., 2012, 2014). For example, Peña-Rodríguez et al. (2014) estimated exogenic Hg accounting for 87% in upper O- and A-horizons in Subantartic forest soils of Tierra del Fuego and 64% in B soil horizons. In Guedron et al. (2006), between 75% and 90% of Hg in French Guiana soils in South America was considered of exogenic origin. Finally, 45% of soil Hg was of estimated exogenic origin in European volcanic soils with naturally enriched Hg background levels (Peña-Rodríguez et al., 2012). Hg isotope studies across different forested sites (Demers et al., 2013; Jiskra et al., 2015; Wang et al., 2017; Zheng et al., 2016) confirm a predominance of Hg^0 from atmospheric deposition as a source to many surface soil layers across forested sites.

PCA using major and trace soil elements from all measured soil horizons highlights that Hg in tundra soils was largely unrelated to other crustal elements (Figure S2). The first and second components of a PCA are plotted in Figure S2. The first component (PC1) has an eigenvalue of 5.9 and explains 46% of the variance in the data set. The second component (PC2) has an eigenvalue of 2.4 and explains 19% of the overall variance in the data set. In PC1, a group of elements including Fe, Al, Ti, Zr, Rb, and Cr were strongly grouped together on the negative loading of this vector. These elements include typical crustal elements (e.g., Ti, Al, and Sr) and hence indicate a crustal (i.e., geogenic) source. Hg is located on the opposite side of this vector, along with OC, and the component explains 46% of the total concentration variance of Hg. These patterns support exogenic sources of Hg dominating in active-layer soils that are strongly associated with OC. While we discussed above that B soil horizons contain 49% geogenic contributions, overall their contribution to soil Hg concentrations across the entire soil profile (particularly in upper layers) remains small. Along PC2, we found a weak association of Hg with Mn and elements including Pb, Zn, and Cu—with this second component showing a much smaller eigenvalue (19% of the concentration variance of Hg). It is possible that Pb, Zn, and Cu—all showing negative loading on PC2 similar to Hg—are indicative of similar source origins, possibly including anthropogenic inputs (Agnan et al., 2015; Carling et al., 2012; Gabrieli et al., 2011; Lamborg et al., 2013). It is important to note, however, that atmospheric cycling of these potentially anthropogenic-derived elements is mainly related to particulate deposition and thus very different to Hg.

3.3. Spatial Variability of Tundra Soil Hg Concentrations

We hypothesized that near-coastal sites may show higher soil Hg concentrations compared to inland sites because of the presence of AMDEs near the Arctic Ocean coasts (Moore et al., 2014; Schroeder & Munthe, 1998; Steffen et al., 2008). AMDEs have been estimated to enhance Hg deposition by up to 325 Mg in the Arctic each year (Ariya et al., 2004; Steffen et al., 2008), although newer studies question the importance of these events for large deposition impacts in the Arctic (Douglas et al., 2012; Obrist et al., 2017) because of significant revolatilization losses after deposition. Figure 4 shows pedogenic horizons, patterns of total Hg concentrations, and OC concentrations of 12 soil pits excavated along an approximately 200 km Dalton Highway transect on the north Alaskan slope (Figure 1), with the northernmost site within 30 km of the Arctic Ocean.

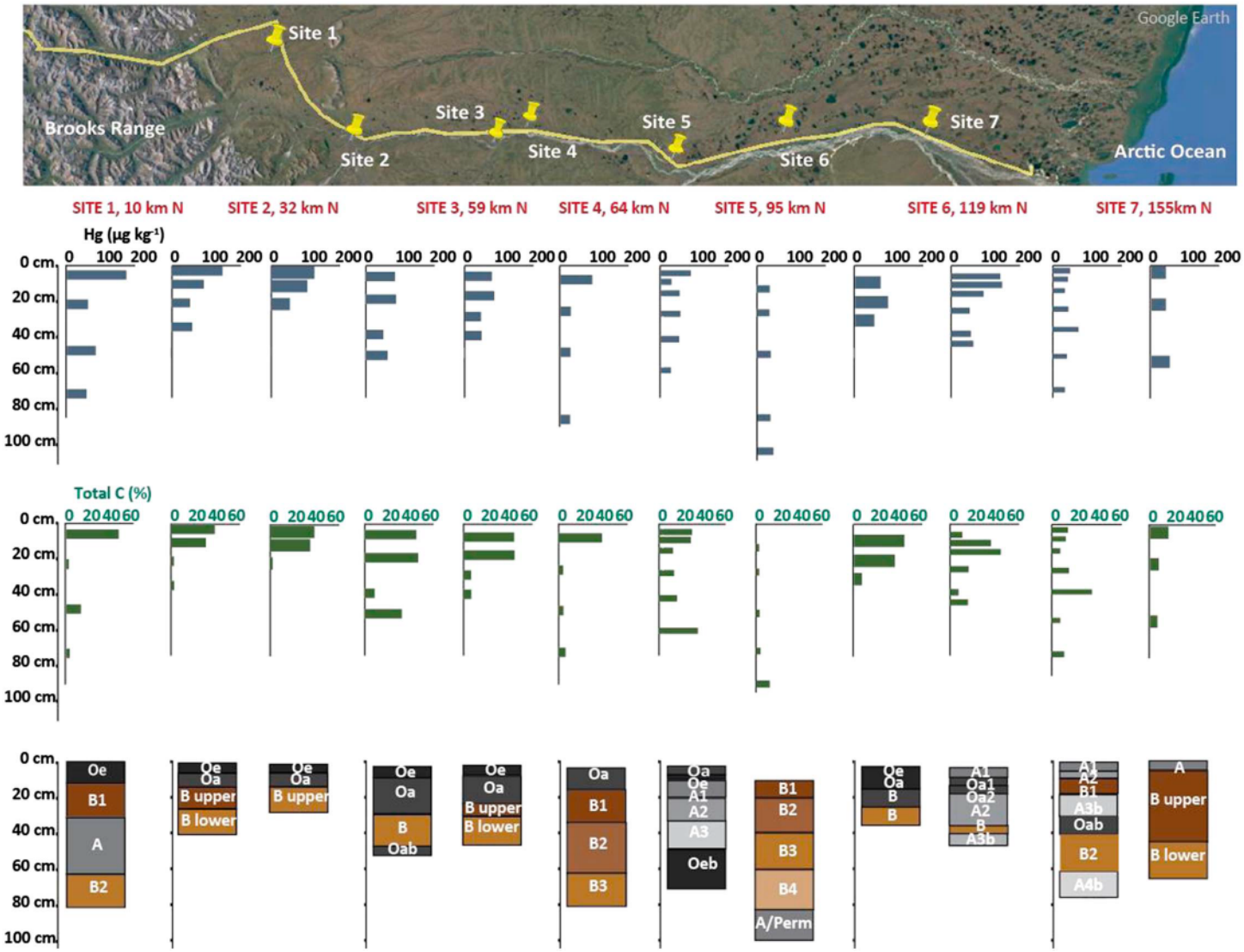

Figure 4. Detailed characterization of 12 soil pits dug at seven sites along the Dalton Highway transect. Location of the seven sites is shown in the top map with proximity to Toolik Field station (km N). Hg concentrations (µg/kg) with depth are shown in the blue vertical bar charts. Total carbon (%) with depth is shown in the green vertical bar charts, and the detailed soil horizon depth profile is shown for each pit. Note that the depth scales (i.e., *y* axis) shown for site 1 apply to all sites.

Across this transect, Hg concentrations also were highest in organic horizons (99 ± 6 µg/kg), followed by A-horizons (65 ± 8 µg/kg), and lowest Hg concentrations were found in B-horizons (45 ± 3 µg/kg). Soil Hg concentrations on average were lower than at Toolik Field Station, by −34% (organic horizons), −41% (A-horizons), and − 48% (B-horizons). We observed a statistically significant linear decline ($P = 0.02$, $r^2 = 0.17$) of tundra soil Hg concentrations with higher latitude along the transect. Hg concentrations decreased northward despite increasing OC concentrations (Figure S3) in mineral soils, so that spatial patterns of Hg and OC distribution were unrelated, in contrast to such a relationship observed elsewhere (Obrist et al., 2011). Although the reasons for this decrease in Hg concentration with latitude are unclear, it may be related to a shorter growing season and lower plant productivity at sites closer to the Arctic Ocean (Narasimhan & Stow, 2010), resulting in lower plant Hg inputs to the soils. In summary, proximity to the coast, and potential higher deposition impacts by AMDEs did not lead to increases in soil Hg concentrations at near-coastal sites compared to inland sites.

An important feature observed along the northern tundra transect was that several pits showed significant buried organic layers from cryoturbation, mixing OM into mineral horizons (Ping et al., 1998). We observed

buried OM in three of the 12 soil pits from sites 3, 5, and 7 (Figure 4). The observed mean Hg concentrations in the buried OM samples, all of which were overlaid by mineral horizons, were 57 μg/kg, or 15% higher, than the concentrations in mineral horizons above. The higher observed Hg concentrations in buried OM were likely a result of mixing surface organic soils with relatively high OC and Hg concentrations deeper in the soil profile. This suggests a potentially important role of cryoturbation for incorporation of atmospherically derived Hg into the profile in tundra soils.

Other tundra sites sampled across Alaska showed similar tundra soil Hg concentrations as observed in northern Alaska. For example, sites at Noatak near the Alaskan west coast showed mean Hg concentrations of 106 ± 13 μg/kg in organic horizons and 53 ± 4 μg/kg in mineral soils (Figure S4). Sites near Denali National Park in central Alaska (Figure S5) showed mean Hg soil concentrations of 91 ± 10 μg/kg in organic horizons. Surprisingly at this site, the highest Hg concentrations were found at deeper depths (>1 m), averaging 109 μg/kg. We associated these higher soil Hg concentrations at greater depth with unusually high OC content (>20%), again indicating the potential importance of cryoturbation for enriching Hg concentrations in deeper soils.

3.4. Active-Layer Hg Pool Sizes in Northern Alaska Arctic Tundra Soils

We measured bulk densities (range: 0.09 to 1.69 g/cm^3) in all sampled soil horizons and calculated the mass per area of Hg contained in the active-layer zone of Arctic tundra soils (multiplying bulk densities by Hg concentrations). Active-layer depth pool sizes of the total 15 soil pits at Toolik Field station and along the Dalton Highway transect sites showed a wide range from 166 to 1,365 g/ha, with a mean pool size of 419 ± 92 g/ha (Figure S6). Hg mass calculated for the Noatak near the Alaskan west coast showed Hg mass with a range of 200 to 355 g/ha. These pool sizes were 34% lower than those measured in northern Alaska, largely because of the shallower depth of active-layer mineral horizons. Finally, the Subarctic tundra site near Denali National Park showed an active-layer pool size of 329 g/ha. Across all sites, Hg located in B-horizons had a mean of 263 ± 47 g/ha and accounted for 62% of the total active-layer soil pool. The mean Hg mass was 126 ± 28 g/ha in A-horizons and 36 ± 6 g/ha in organic horizons. A major reason for high Hg mass in deeper soil horizons are their high bulk densities (e.g., bulk densities in B-horizons are 4-to-5 times higher than organic horizon bulk densities). Not surprisingly, Hg mass positively correlated with depth of sampled mineral horizons (P = 0.01), explaining 45% of the variance in Hg mass across these soil pits. Compared to Hg mass in these Arctic tundra soils, mass estimates in temperate forest areas generally show smaller pool sizes, in the range of 120 to 170 g/ha in eastern Germany (Schwesig et al., 1999), 213 g/ha in the northeastern United States (Yu et al., 2014), 53 g/ha in mineral soils of a Minnesota forest (Grigal et al., 2000), and 12 to 80 g/ha in Swedish boreal forests (Kronberg, Drott, et al., 2016). Although comparisons across sites are challenging because different studies reference results to different soil depths, remote Arctic tundra soils show some of the highest Hg pools in soils compared to most temperate soils.

As discussed in section 3.1, we hypothesize that buildup of the observed Hg pools in the active layer of tundra soils is in large part because of long-term atmospheric deposition that occurred over thousands of years. The following coarse mass balance estimation supports this notion. If we use the modern total atmospheric deposition flux we recently measured at Toolik field station (9.2 $\mu g \cdot m^{-2} \cdot year^{-1}$; Obrist et al., 2017) and assume this flux occurred for the last 250 years, this would amount to a mass of 2.3 mg/m^2 (200 years × 9.2 $\mu g \cdot m^{-2} \cdot year^{-1}$). If we assume a preindustrial deposition of approximately one third of the modern deposition flux (Biester et al., 2007; Enrico et al., 2017; Lindberg et al., 2007), the additional deposition to 7,200-year-old soils would amount to 21.5 mg/m^2 (6,950 years × 3.1 $\mu g \cdot m^{-2} \cdot year^{-1}$), resulting in a total deposition load of 23.8 mg/m^2, or 238 g/ha. This coarse estimate is at the lower range of estimated soil Hg pool sizes we found in active-layer tundra soils (166 to 1,365 g/ha; also note, however, that B-horizons contain up to 40% of geogenic sources). These calculations suggest that most Hg in Arctic tundra soils (~90%) may be derived from preindustrial deposition, although there are several important caveats to this coarse mass balance estimate. For example, studies show that peak atmospheric Hg(0) concentrations, in particular near Europe and the United States, were much higher in the 1970s (Enrico et al., 2017; Fain et al., 2009) so that peak deposition rates in the twentieth century may have been substantially higher than measured in the last few years. In addition, peak atmospheric Hg(0) concentrations may have been up to 15 times larger than preindustrial levels, further shifting the ratio of modern to prehistoric Hg deposition toward contributions of modern anthropogenic sources. Finally, this estimate

Table 1
Arctic Tundra Active-Layer Soil Hg Pool Calculations for the Upper 100 cm of Permafrost

Arctic soils (median)	Median Hg (μg/kg)	Median C (%)	Hg:C (μg/kg)	Carbon pool (Pg)[a]	Median Hg pool size (g)	Median Hg pool size (Gg)
Organic soils, 0–30 cm	40	42	274	217	2.58E + 10	26
Mineral soils, 30–100 cm	40	6	621	255	1.58E + 11	158
Number of samples	478	295	295			
Arctic soils (37.5th %)	37.5th % Hg (μg/kg)	37.5th % C (%)	Hg:C (μg/kg)	Carbon pool (Pg)[a]	37.5th Hg pool size (g)	37.5th Hg pool size (Gg)
Organic soils, 0–30 cm	32	41	95	217	2.06E + 10	21
Mineral soils, 30–100 cm	31	4	450	255	1.15E + 11	115
Number of samples	478	295	295			
Arctic soils (62.5th %)	62.5th % Hg (μg/kg)	62.5th % C (%)	Hg:C (μg/kg)	Carbon pool (Pg)[a]	62.5th Hg pool size (g)	62.5th Hg pool size (Gg)
Organic soils, 0–30 cm	57	43	193	217	4.19E + 10	42
Mineral soils, 30–100 cm	50	7	911	255	2.32E + 112	232
Number of samples	478	295	295			

Note. This table provides a compiled data set containing 478 measurements based on 15 published studies of soil Hg concentrations (ug/kg), carbon (%), and Hg:C ratios (ug/kg) in Arctic locations. Summary statistics were used to calculate medians and percentiles (37.5th and 62.5th) for Hg, C, and Hg:C ratios. Carbon pool estimates from Hugelius et al. (2014) were multiplied by the upper, organic soil (0–30 cm depth) and lower, mineral soil (30–100 cm depth) Hg:C ratios to provide a 37.5th, median, and 62.5th Hg pool size stored in Arctic tundra soils.
[a]Used carbon pool estimates for 0- to 30- and 30- to 100-cm depth of active layer permafrost from Hugelius et al. (2014).

ignores mobilization of Hg from these soils. Still, these estimates strongly suggest that long-term deposition sources must be present to account for the high soil Hg pools we observed across Arctic tundra soils.

We collected a data set of Hg concentrations in soils of Arctic and boreal locations based on 33 published studies (Table 1 and the supporting information). Out of 478 soil data points found in the literature reporting Hg concentrations in Arctic tundra soils, concentrations ranged from 1 to 420 μg/kg with a median of 40 μg/kg and a mean of 57 μg/kg. The concentration range of the middle 25% of data (i.e., 37.5th to 62.5th percentiles) was 30 to 52 μg/kg. Soil Hg concentrations showed similar patterns in the upper 30 cm and lower 30–100 cm, both with median values of 40 μg/kg. Soil Hg:C ratios showed a median of 274 μg/kg and a range of 25 to 833 μg/kg for the upper 30 cm of the soil profile, with a median of 621 μg/kg for the mineral soil layers. Based on these Hg:C ratios, we used Arctic soil C inventories from Hugelius et al. (2014), who estimated OC pools in global Arctic tundra soils for the upper 30 cm (217 Pg) and upper 100 cm (472 Pg). Note that Schuster et al. (2018) reported close correlations between soil organic C and soil Hg (for 80% of the data: r^2 of 0.98 for C content <10% and r^2 of 0.56 for >10%), so additional variance in scaling up Hg pools based on C inventories are due to imperfect Hg-to-C relationships). Using this approach, we estimated a median Arctic tundra active-layer soil Hg pool for the upper 30 cm of 26 Gg with a range (37.5th to 62.5th percentile range Hg:C ratios) of 21 to 42 Gg. Similarly, using the Hg:C ratios of mineral soils (median and 25% middle range) and Hugelius et al.'s (2014) estimate for OC pool of 255 Pg for soil depths of 30–100 cm, we estimated a median active-layer Arctic Hg pool of 158 Gg and a range of 115 to 232 Gg. Hence, total active-layer soil Hg pool sizes for the upper 100 cm of Arctic tundra soils would account for 184 Gg with a range of 136 to 274 Gg. These estimates are a further refinement of the global tundra soil Hg pool size first estimated by Obrist et al. (2017) of 143 Gg. We also estimate pool sizes in the boreal zone (see the supporting information). Scaling up boreal zone Hg pools may be even more challenging because of the large variability in ecosystem types and soil structure (Chapin et al., 2000). Using a similar approach, however, based on boreal-zone soil C inventories (703 Pg from Kasischke, 2000) and Hg:C ratios and ranges for a boreal data set (supporting information), we estimated a median global boreal Hg pool size of 224 Gg (range: 183 to 310 Gg). Together, northern tundra and boreal soils would contain a pool size of 408 (and range of 319 to 584) Gg of Hg.

Recently, Schuster et al. (2018) estimated NH permafrost soils (up to depths of 3 m) to contain 1,656 Gg of Hg of which 793 Gg is stored in perennially frozen layers with 863 Gg in upper soils of permafrost and boreal zones. These measurements were based on 13 permafrost cores across Alaska and 11,000 measurements of which roughly half came from temperate, nonpermafrost sites in North American and Eurasia. Our combined estimate for Hg pools of 408 Gg for the top 100 cm of boreal and Arctic soils is about half of what Schuster et al. (2018) estimated was stored within upper soils (863 Gg). Despite this difference, both

studies support large magnitudes and role of Arctic soils as globally important storage pools for Hg. For example, the estimates for tundra soil active-layer Hg pools are very large compared to previous estimates of global soil Hg mass based on temperate studies (~240 Gg, Smith-Downey et al., 2010; ~300 Gg, Hararuk et al., 2013; and 250 to 1,000 Gg with a best estimate of 500 Gg; Amos et al., 2015), and our estimate suggests that overall, global soil Hg pools may be greatly underestimated. The northern soil Hg pool estimates also are large compared to previous estimates of Hg in boreal upper soils by Friedli et al. (2007) of 14 to 40 Gg.

A critical concern of high Arctic soil Hg pools is their potential to contribute Hg to river runoff and Arctic Ocean input via coastal erosion (Reyes & Lougheed, 2015; Schuur et al., 2011). Three of the 10 largest rivers in the world are in the Eurasian Arctic and Subarctic, draining into the small and shallow Arctic Ocean (Vörösmarty et al., 2000). Circumpolar rivers flowing into the Arctic Ocean account for 11% of all freshwater inputs to the world's oceans. Yet we currently do not have a good understanding of the factors and processes impacting Hg mobilization in upland soils. A preliminary analysis of Hg mobility from active-layer and permafrost tundra soils showed soil-solution Hg concentrations (dissolved fraction) in the range of 3 ± 0.4 ng/L, higher than commonly reported background river Hg concentrations (Schuster et al., 2011). We also observe higher potential for Hg mobilization in samples from active-layer soils compared to deeper permafrost samples (3.2 ng/L versus 0.9 ng/L). While a process-based understanding of Hg mobilization from tundra soils is not yet feasible, river studies clearly show that upland soils serve as major sources of sediments, OC, and Hg (Dittmar & Kattner, 2003). For example, the Mackenzie River, draining through the Canadian Arctic and Subarctic, shows a sevenfold increase in particulate and dissolved Hg levels during peak flow season mobilizing terrestrial Hg sources (Leitch et al., 2007). Estimates of total delivery of Hg to the Arctic Ocean include estimates of 5–10 Mg/year by Outridge et al. (2008) and Amos et al. (2014) to 46 Mg/year by Zhang et al. (2015) and up to 95 Mg/year by Fisher et al. (2012). All of these estimates indicate northern soils to be major sources of Hg to the Arctic Ocean with consequences and biological impacts to humans and Arctic wildlife that rely on Arctic Ocean food sources (AMAP, 2009).

4. Summary and Conclusions

Tundra soil investigations spanning 11 tundra sites on the north slope of Alaska and additional sites in the western Arctic and the Subarctic provided evidence of high soil Hg concentrations and pool sizes across the remote Alaskan Arctic and Subarctic. While organic horizons showed Hg concentrations comparable to temperate soils, mineral horizon concentrations were 2-to-5 times higher than those observed in temperate areas and contained 75% of total Hg mass stored in tundra soil. Sources of high soil Hg concentrations—assessed by mass balance estimates, geochemical tracers, and stable Hg isotopes—were mainly derived from atmospheric deposition of Hg, particularly elemental Hg^0 that is ubiquitous in the global atmosphere. In addition, lack of reemissions and long-term accumulation of Hg in old soils across many millennia have allowed sequestration of large Hg pools in active layers (upper 100 cm) of tundra soils. Northern tundra and boreal soils represent a globally important storage pool of Hg, containing 408 Gg (range of 319 to 584 Gg). Concerns regarding large tundra soil Hg pools are their potential mobilization induced by climate change (Schuster et al., 2018). Such changes—including increased thermokarst occurrences and soil degradation (Jorgenson & Osterkamp, 2005) as well as warming-induced slumping along river banks (Lantz & Kokelj, 2008) and coastal areas (Lantuit & Pollard, 2008)—lead to increased soil export. Other studies found increased active-layer depths (Osterkamp, 2005; Åkerman & Johansson, 2008), increased carbon losses (Kane, 2012), changes in water-table levels (Klaminder et al., 2008), and infiltration of water deeper into mineral soil profiles (Carey et al., 2013; Quinton et al., 2005). Finally, increased occurrence of wildfires has the ability to remobilize Hg from soils to the atmosphere (Turetsky et al., 2006, 2011).

Acknowledgments

The data used for this study are listed in the figures, tables, and supporting information. We thank Olivia Dillon for help with sample preparation and analysis; Jonathan ODonnell and George Aiken for collecting samples in the Noatak National Preserve; Ted Schuur, Marguerite Mauritz, and Shannon Coykendall for arranging accommodations to sample near Denali National Park and for assistance with samples from 8 Mile Lake Study area; Chien-Lu Ping for his insight into tundra soils and help with sample collection along the Dalton Highway transect; Roger Kreidberg for editorial help; and Ruben Kretzschmar and Kurt Barmettler for inorganic carbonate analysis of soil samples. This study was funded by a grant from the U.S. National Science Foundation Office of Polar Programs to PIs Daniel Obrist and Detlev Helmig (1304305 and 1739567) with additional support by a U.S. Department of Energy grant (DE-SC0014275). Martin Jiskra received funding from the European Union's Horizon 2020 research and innovation program under the Marie Sklodowska-Curie grant agreement 657195.

References

Agnan, Y., Sejalon-Delmas, N., Claustres, A., & Probst, A. (2015). Investigation of spatial and temporal metal atmospheric deposition in France through lichen and moss bioaccumulation over one century. *Science of the Total Environment, 529*, 285–296. https://doi.org/10.1016/j.scitotenv.2015.05.083

Åkerman, H. J., & Johansson, M. (2008). Thawing permafrost and thicker active layers in subarctic Sweden. *Permafrost and Periglacial, 19*(3), 279–292. https://doi.org/10.1002/ppp.626

AMAP (2009). *AMAP Assessment 2009: Human Health in the Arctic* (xiv+254 pp.). Oslo, Norway: Arctic Monitoring and Assessment Programme (AMAP).

AMAP (2011). AMAP Assessment 2011: Mercury in the Arctic (xiv + 193 pp.). Oslo, Norway: Arctic Monitoring and Assessment Programme (AMAP).
Amos, H. M., Jacob, D. J., Kocman, D., Horowitz, H. M., Zhang, Y., Dutkiewicz, S., et al. (2014). Global biogeochemical implications of mercury discharges from rivers and sediment burial. *Environmental Science & Technology*, *48*(16), 9514–9522. https://doi.org/10.1021/es502134t
Amos, H. M., Sonke, J. E., Obrist, D., Robins, N., Hagan, N., Horowitz, H. M., et al. (2015). Observational and modeling constraints on global anthropogenic enrichment of mercury. *Environmental Science & Technology*, *49*(7), 4036–4047. https://doi.org/10.1021/es5058665
Ariya, P. A., Dastoor, A. P., Amyot, M., Schroeder, W. H., B, L., Anlauf, K., et al. (2004). The Arctic: A sink for mercury. *Tellus B*, *56*(5), 397–403. https://doi.org/10.3402/tellusb.v56i5.16458
Ayotte, P., Weber, J., Levallois, P., Bruneau, S., Dewailly, É., & Lebel, G. (2001). Exposure of the Inuit population of Nunavik (Arctic Québec) to lead and mercury. *Archives of Environmental Health*, *56*(4), 350–357.
Bailey, R. G. (2014). *Ecoregions: The ecosystem geography of the oceans and continents*. New York: Springer. https://doi.org/10.1007/978-1-4939-0524-9
Ball, D. F. (1964). Loss-on-ignition as an estimate of organic matter and organic carbon in non-calcareous soils. *Journal of Soil Science*, *15*(1), 84–92. https://doi.org/10.1111/j.1365-2389.1964.tb00247.x
Biester, H., Bindler, R., Martinez-Cortizas, A., & Engstrom, D. R. (2007). Modeling the past atmospheric deposition of mercury using natural archives. *Environmental Science & Technology*, *41*(14), 4851–4860. https://doi.org/10.1021/es0704232
Borden, P. W., Ping, C. L., McCarthy, P. J., & Naidu, S. (2010). Clay mineralogy in arctic tundra gelisols, northern Alaska. *Soil Science Society of America Journal*, *74*(2), 580–592. https://doi.org/10.2136/sssaj2009.0187
Carey, S. K., Boucher, J. L., & Duarte, C. M. (2013). Inferring groundwater contributions and pathways to streamflow during snowmelt over multiple years in a discontinuous permafrost subarctic environment (Yukon, Canada). *Hydrogeology Journal*, *21*(1), 67–77. https://doi.org/10.1007/s10040-012-0920-9
Carling, G. T., Fernandez, D. P., & Johnson, W. P. (2012). Dust-mediated loading of trace and major elements to Wasatch Mountain snowpack. *Science of the Total Environment*, *432*, 65–77. https://doi.org/10.1016/j.scitotenv.2012.05.077
Chapin, F. S., Mcguire, A. D., Randerson, J., Pielke, R., Baldocchi, D., Hobbie, S. E., et al. (2000). Arctic and boreal ecosystems of western North America as components of the climate system. *Global Change Biology*, *6*(S1), 211–223. https://doi.org/10.1046/j.1365-2486.2000.06022.x
Chow, J. C., Watson, J. G., Houck, J. E., Pritchett, L. C., Fred Rogers, C., Frazier, C. A., et al. (1994). A laboratory resuspension chamber to measure fugitive dust size distributions and chemical compositions. *Atmospheric Environment*, *28*(21), 3463–3481. https://doi.org/10.1016/1352-2310(94)90005-1
Dastoor, A. P., & Durnford, D. A. (2014). Arctic Ocean: Is it a sink or a source of atmospheric mercury? *Environmental Science & Technology*, *48*(3), 1707–1717. https://doi.org/10.1021/es404473e
Demers, J. D., Blum, J. D., & Zak, D. R. (2013). Mercury isotopes in a forested ecosystem: Implications for air-surface exchange dynamics and the global mercury cycle. *Global Biogeochemical Cycles*, *27*, 222–238. https://doi.org/10.1002/gbc.20021
Dietz, R., Riget, F., Born, E. W., Sonne, C., Grandjean, P., Kirkegaard, M., et al. (2006). Trends in mercury in hair of Greenlandic polar bears (*Ursus maritimus*) during 1892–2001. *Environmental Science & Technology*, *40*(4), 1120–1125.
Dittmar, T., & Kattner, G. (2003). The biogeochemistry of the river and shelf ecosystem of the Arctic Ocean: A review. *Marine Chemistry*, *83*(3–4), 103–120. https://doi.org/10.1016/S0304-4203(03)00105-1
Douglas, T. A., Loseto, L. L., MacDonald, R. W., Outridge, P., Dommergue, A., Poulain, A., et al. (2012). The fate of mercury in Arctic terrestrial and aquatic ecosystems: A review. *Environment and Chemistry*, *9*(4), 321. https://doi.org/10.1071/EN11140
Dray, S., & Dufour, A.-B. (2007). The ade4 package: Implementing the duality diagram for ecologists. *Journal of Statistical Software*, *22*(4). https://doi.org/10.18637/jss.v022.i04
Drevnick, P. E., Cooke, C. A., Barraza, D., Blais, J. M., Coale, K. H., Cumming, B. F., et al. (2016). Spatiotemporal patterns of mercury accumulation in lake sediments of western North America. *Science of the Total Environment*, *568*, 1157–1170. https://doi.org/10.1016/j.scitotenv.2016.03.167
Emmerton, C. A., Graydon, J. A., Gareis, J. A., St Louis, V. L., Lesack, L. F., Banack, J. K., et al. (2013). Mercury export to the Arctic Ocean from the Mackenzie River, Canada. *Environmental Science & Technology*, *47*(14), 7644–7654. https://doi.org/10.1021/es400715r
Enrico, M., Roux, G. L., Heimbrger, L. E., Van Beek, P., Souhaut, M., Chmeleff, J., & Sonke, J. E. (2017). Holocene atmospheric mercury levels reconstructed from peat bog mercury stable isotopes. *Environmental Science & Technology*, *51*(11), 5899–5906. https://doi.org/10.1021/acs.est.6b05804
EPA-U (1998a). *Method 7473 (SW-846): Mercury in Solids and Solutions by Thermal Decomposition, Amalgamation, and Atomic Absorption Spectrophotometry*, Revision 0. Washington, DC.
EPA-U (1998b). *Method 7473 (SW-846): Method 1630, Methyl mercury in water by distillation, aqueous ethylation, purge and trap, and CVAFS*. Washington, DC.
EPA-U (2002). *Method 1631, revision E: Mercury in water by oxidation, purge and trap, and cold vapor atomic fluorescence spectrometry*. Washington, DC: U.S. Environmental Protection Agency.
Fain, X., Ferrari, C. P., Dommergue, A., Albert, M. R., Battle, M., Severinghaus, J., et al. (2009). Polar firn air reveals large-scale impact of anthropogenic mercury emissions during the 1970s. *Proceedings of the National Academy of Sciences of the United States of America*, *106*(38), 16,114–16,119. https://doi.org/10.1073/pnas.0905117106
Fisher, J. A., Jacob, D. J., Soerensen, A. L., Amos, H. M., Steffen, A., & Sunderland, E. M. (2012). Riverine source of Arctic Ocean mercury inferred from atmospheric observations. *Nature Geoscience*, *5*(7), 499–504. https://doi.org/10.1038/ngeo1478
Fitzgerald, W. F., Engstrom, D. R., Lamborg, C. H., Tseng, C. M., Balcom, P. H., & Hammerschmidt, C. R. (2005). Modern and historic atmospheric mercury fluxes in northern Alaska: Global sources and Arctic depletion. *Environmental Science & Technology*, *39*(2), 557–568. https://doi.org/10.1021/es049128x
Friedli, H. R., Radke, L. F., Payne, N. J., McRae, D. J., Lynham, T. J., & Blake, T. W. (2007). Mercury in vegetation and organic soil at an upland boreal forest site in Prince Albert National Park, Saskatchewan, Canada. *Biogeosciences*, *112*(G1), G01004.
Gabrieli, J., Cozzi, G., Vallelonga, P., Schwikowski, M., Sigl, M., Eickenberg, J., et al. (2011). Contamination of alpine snow and ice at Colle Gnifetti, Swiss/Italian Alps, from nuclear weapons tests. *Atmospheric Environment*, *45*(3), 587–593. https://doi.org/10.1016/j.atmosenv.2010.10.039
Garrett, R. G. (2013). The 'rgr' package for the R Open Source statistical computing and graphics environment—A tool to support geochemical data interpretation. *Journal of Electronics*. https://doi.org/10.1144/geochem2011-106
Givelet, N., Roos-Barraclough, F., Goodsite, M. E., Cheburkin, A. K., & Shotyk, W. (2004). Atmospheric mercury accumulation rates between 5900 and 800 calibrated years BP in the High Arctic of Canada recorded by peat hummocks. *Environmental Science & Technology*, *38*(19), 4964–4972. https://doi.org/10.1021/es035293l

Grigal, D. F. (2003). Mercury sequestration in forests and peatlands: A review. *Journal of Environmental Quality*, *32*(2), 393–405. https://doi.org/10.2134/jeq2003.3930

Grigal, D. F., Kolka, R. K., Fleck, J. A., & Nater, E. A. (2000). Mercury budget of an upland-peatland watershed. *Biogeochemistry*, *50*(1), 95–109. https://doi.org/10.1023/A:1006322705566

Guedron, S., Grimaldi, C., Chauvel, C., Spadini, L., & Grimaldi, M. (2006). Weathering versus atmospheric contributions to mercury concentrations in French Guiana soils. *Applied Geochemistry*, *21*(11), 2010–2022. https://doi.org/10.1016/j.apgeochem.2006.08.011

Hammerschmidt, C. R., Fitzgerald, W. F., Lamborg, C. H., Balcom, P. H., & Tseng, C. M. (2006). Biogeochemical cycling of methylmercury in lakes and tundra watersheds of Arctic Alaska. *Environmental Science & Technology*, *40*(4), 1204–1211. https://doi.org/10.1021/es051322b

Hararuk, O., Obrist, D., & Luo, Y. (2013). Modelling the sensitivity of soil mercury storage to climate-induced changes in soil carbon pools. *Biogeosciences*, *10*(4), 2393–2407. https://doi.org/10.5194/bg-10-2393-2013

Harris, R. C., Rudd, J. W. M., Amyot, M., Babiarz, C. L., Beaty, K. G., Blanchfield, P. J., et al. (2007). Whole-ecosystem study shows rapid fish-mercury response to changes in mercury deposition. *Proceedings of the National Academy of Sciences of the United States of America*, *104*(42), 16,586–16,591. https://doi.org/10.1073/pnas.0704186104

Henning, T. A., Brezonik, P. L., & Engstrom, D. E. (1989). Historical and areal deposition of mercury in NE Minnesota and Northern Wisconsin Lakes, Minnesota Pollution Control Agency.

Hojdova, M., Rohovec, J., Chrastny, V., Penizek, V., & Navratil, T. (2015). The influence of sample drying procedures on mercury concentrations analyzed in soils. *Bulletin of Environmental Contamination and Toxicology*, *94*(5), 570–576. https://doi.org/10.1007/s00128-015-1521-9

Hugelius, G., Strauss, J., Zubrzycki, S., Harden, J. W., Schuur, E. A. G., Ping, C. L., et al. (2014). Estimated stocks of circumpolar permafrost carbon with quantified uncertainty ranges and identified data gaps. *Biogeosciences*, *11*, 6573–6593.

Jaeglé L. 2010. Atmospheric long-range transport and deposition of mercury to Alaska, A report to the Alaska Department of Environmental Conservation, May 10, 2010.

Jiskra, M., Wiederhold, J. G., Skyllberg, U., Kronberg, R. M., Hajdas, I., & Kretzschmar, R. (2015). Mercury deposition and re-emission pathways in boreal forest soils investigated with Hg isotope signatures. *Environmental Science & Technology*, *49*(12), 7188–7196. https://doi.org/10.1021/acs.est.5b00742

Jorgenson, M. T., & Osterkamp, T. E. (2005). Response of boreal ecosystems to varying modes of permafrost degradation. *Canadian Journal of Forest Research*, *35*(9), 2100–2111. https://doi.org/10.1139/x05-153

Kane, E. S. (2012). Squeezing the arctic carbon balloon: Ecosystem carbon storage. *Nature Climate Change*, *2*(12), 841–842. https://doi.org/10.1038/nclimate1764

Kasischke, E. S. (2000). Boreal ecosystems in the global carbon cycle. In E. S. Kasischke & B. J. Stocks (Eds.), *Fire, Climate Change and Carbon Cycling in the Boreal Forest*, *Ecological Studies Series* (chap. 1, pp. 19–30). New York: Springer-Verlag. https://doi.org/10.1007/978-0-387-21629-4_2

Klaminder, J., Yoo, K., Giesler, R., Teknisk-naturvetenskapliga, f., Umeå, u., & ekologi, m. o. g. l. f. (2009). Soil carbon accumulation in the dry tundra: Important role played by precipitation. *Journal of Geophysical Research*, *114*, G04005. https://doi.org/10.1029/2009JG000947

Klaminder, J., Yoo, K., Rydberg, J., & Giesler, R. (2008). An explorative study of mercury export from a thawing palsa mire. *Journal of Geophysical Research*, *113*, G04034. https://doi.org/10.1029/2008JG000776

Kronberg, R.-M., Drott, A., Jiskra, M., Wiederhold, J. G., Björn, E., & Skyllberg, U. (2016). Forest harvest contribution to boreal freshwater methyl mercury load. *Global Biogeochemical Cycles*, *30*, 825–843. https://doi.org/10.1002/2015GB005316

Kronberg, R.-M., Jiskra, M., Wiederhold, J. G., Björn, E., & Skyllberg, U. (2016). Methyl mercury formation in killslope soils of boreal forests: The role of forest harvest and anaerobic microbes. *Environmental Science & Technology*, *50*(17), 9177–9186. https://doi.org/10.1021/acs.est.6b00762

Laliberté, C., Dewailly, É., Gingras, S., Ayotte, P., Weber, J., Sauvé, L., & Benedetti, J. (1992). In J. P. Vernet (Ed.), *Mercury contamination in fishermen of the lower north shore of the Gulf of St-Lawrence (Québec, Canada)*, *Trace Metals Other* (Vol. 15, p. 28). Amsterdam: Elsevier Science Publishers.

Lamborg, C. H., Engstrom, D. R., Fitzgerald, W. F., & Balcom, P. H. (2013). Apportioning global and non-global components of mercury deposition through Pb-210 indexing. *Science of the Total Environment*, *448*, 132–140. https://doi.org/10.1016/j.scitotenv.2012.10.065

Lantuit, H., & Pollard, W. H. (2008). Fifty years of coastal erosion and retrogressive thaw slump activity on Herschel Island, southern Beaufort Sea, Yukon Territory, Canada. *Geomorphology*, *95*(1-2), 84–102. https://doi.org/10.1016/j.geomorph.2006.07.040

Lantz, T. C., & Kokelj, S. V. (2008). Increasing rates of retrogressive thaw slump activity in the Mackenzie Delta region, NWT, Canada. *Geophysical Research Letters*, *35*, L06502. https://doi.org/10.1029/2007GL032433

Larcher, W. (1995). *Physiological plant ecology: Ecophysiology and stress physiology of functional groups*. New York; Berlin: Springer-Verlag. https://doi.org/10.1007/978-3-642-87851-0

Lee, H., Schuur, E. A. G., & Vogel, J. G. (2010). Soil CO_2 production in upland tundra where permafrost is thawing. *Journal of Geophysical Research – Biogeosciences*, *115*, G01009. https://doi.org/10.1029/2008JG000906

Lee, R. E. Jr. (2015). In J. E. Hobbie & G. W. Kling (Eds.), *Alaska's changing Arctic: Ecological consequences for tundra, streams, and lakes*, (p. 1170). Middletown: American Library Association CHOICE.

Leitch, D. R., Carrie, J., Lean, D., Macdonald, R. W., Stern, G. A., & Wang, F. Y. (2007). The delivery of mercury to the Beaufort Sea of the Arctic Ocean by the Mackenzie River. *Science of the Total Environment*, *373*(1), 178–195. https://doi.org/10.1016/j.scitotenv.2006.10.041

Lindberg, S., Bullock, R., Ebinghaus, R., Engstrom, D., Feng, X. B., Fitzgerald, W., et al. (2007). A synthesis of progress and uncertainties in attributing the sources of mercury in deposition. *Ambio*, *36*(1), 19–33. https://doi.org/10.1579/0044-7447(2007)36[19:ASOPAU]2.0.CO;2

Lindqvist, O., Johansson, K., Bringmark, L., Timm, B., Aastrup, M., Andersson, A., et al. (1991). Mercury in the Swedish environment—Recent research on causes, consequences and corrective methods. *Water, Air, and Soil Pollution*, *55*(1–2), xi–261.

Lorey, P. D. C. T. (1999). Historical trends of mercury deposition in Adirondack lakes. *Environmental Science & Technology*, *33*(5), 718–722. https://doi.org/10.1021/es9800277

MacMillan, G. A., Girard, C., Chetelat, J., Laurion, I., & Amyot, M. (2015). High methylmercury in Arctic and subarctic ponds is related to nutrient levels in the warming eastern Canadian Arctic. *Environmental Science & Technology*, *49*(13), 7743–7753. https://doi.org/10.1021/acs.est.5b00763

Michaelson, G. J., Ping, C.-L., & Clark, M. (2013). Soil pedon carbon and nitrogen data for Alaska: An analysis and update. *Journal of Soil Science*, *3*(2), 132–142.

Mierle, G., & Ingram, R. (1991). The role of humic substances in the mobilization of mercury from watersheds. *Water, Air, and Soil Pollution*, *56*(1), 349–357. https://doi.org/10.1007/BF00342282

Moore, C. W., Obrist, D., Steffen, A., Staebler, R. M., Douglas, T. A., Richter, A., & Nghiem, S. V. (2014). Convective forcing of mercury and ozone in the arctic boundary layer induced by leads in sea ice. *Nature*, *506*(7486), 81–84. https://doi.org/10.1038/nature12924

Narasimhan, R., & Stow, D. (2010). Daily MODIS products for analyzing early season vegetation dynamics across the North Slope of Alaska. *Remote Sensing of Environment*, *114*(6), 1251–1262. https://doi.org/10.1016/j.rse.2010.01.017

Natali, S. M., Schuur, E. A. G., Webb, E. E., Pries, C. E. H., & Crummer, K. G. (2014). Permafrost degradation stimulates carbon loss from experimentally warmed tundra. *Ecology*, *95*(3), 602–608. https://doi.org/10.1890/13-0602.1

Obrist, D. (2012). Mercury distribution across 14 U.S. forests. Part II: Patterns of methyl mercury concentrations and areal mass of total and methyl mercury. *Environmental Science & Technology*, *46*(11), 5921–5930. https://doi.org/10.1021/es2045579

Obrist, D., Agnan, Y., Jiskra, M., Hedge, C., Colegrove, D., Hueber, J., et al. (2017). Tundra uptake of atmospheric elemental mercury drives Arctic mercury pollution. *Nature*, *547*(7662), 201–204. https://doi.org/10.1038/nature22997

Obrist, D., Johnson, D. W., Lindberg, S. E., Luo, Y., Hararuk, O., Bracho, R., et al. (2011). Mercury distribution across 14 U.S. forests. Part I: Spatial patterns of concentrations in biomass, litter, and soils. *Environmental Science & Technology*, *45*(9), 3974–3981. https://doi.org/10.1021/es104384m

Obrist, D., Pearson, C., Webster, J., Kane, T., Lin, C.-J., Aiken, G. R., & Alpers, C. N. (2016). A synthesis of terrestrial mercury in the western United States: Spatial distribution defined by land cover and plant productivity. *Science of the Total Environment*, *568*, 522–535. https://doi.org/10.1016/j.scitotenv.2015.11.104

Osterkamp, T. E. (2005). The recent warming of permafrost in Alaska. *Global and Planetary Change*, *49*(3–4), 187–202. https://doi.org/10.1016/j.gloplacha.2005.09.001

Outridge, P. M., Hobson, K. A., McNeely, R., & Dyke, A. (2002). A comparison of modern and pre-industrial levels of mercury in the teeth of beluga in the Mackenzie Delta, Northwest Territories, and walrus at Igloolik, Nunavut, Canada. *Arctic*, *55*(2), 123–132.

Outridge, P. M., Macdonald, R. W., Wang, F., Stern, G. A., & Dastoor, A. P. (2008). A mass balance inventory of mercury in the Arctic Ocean. *Environment and Chemistry*, *5*(2), 89–111. https://doi.org/10.1071/EN08002

Peña-Rodríguez, S., Pontevedra-Pombal, X., Fernández-Calviño, D., Taboada, T., Arias-Estévez, M., Martínez-Cortizas, A., et al. (2012). Mercury content in volcanic soils across Europe and its relationship with soil properties. *Journal of Soils and Sediments*, *12*(4), 542–555. https://doi.org/10.1007/s11368-011-0468-7

Peña-Rodríguez, S., Pontevedra-Pombal, X., Gayoso, E. G.-R., Moretto, A., Mansilla, R., Cutillas-Barreiro, L., et al. (2014). Mercury distribution in a toposequence of subantarctic forest soils of Tierra del Fuego (Argentina) as consequence of the prevailing soil processes. *Geoderma*, *232–234*, 130–140.

Ping, C. L., Bockheim, J. G., Kimble, J. M., Michaelson, G. J., & Walker, D. A. (1998). Characteristics of cryogenic soils along a latitudinal transect in Arctic Alaska. *Journal of Geophysical Research*, *103*(D22), 28,917–28,928. https://doi.org/10.1029/98JD02024

Ping, C. L., & Moore, J. P. (1993). Soil classification and climatic zones of Alaska. In *Proceedings of the Sixth International Conference on Permafrost* (Vol. 1).

Quinton, W. L., Shirazi, T., Carey, S. K., & Pomeroy, J. W. (2005). Soil water storage and active-layer development in a sub-alpine tundra hillslope, southern Yukon Territory, Canada. *Permafrost and Periglacial*, *16*(4), 369–382. https://doi.org/10.1002/ppp.543

Reyes, F. R., & Lougheed, V. L. (2015). Rapid nutrient release from permafrost thaw in Arctic aquatic ecosystems. *Arctic, Antarctic, and Alpine Research*, *47*(1), 35–48. https://doi.org/10.1657/AAAR0013-099

Rydberg, J., Klaminder, J., Rosen, P., & Bindler, R. (2010). Climate driven release of carbon and mercury from permafrost mires increases mercury loading to sub-arctic lakes. *Science of the Total Environment*, *408*(20), 4778–4783. https://doi.org/10.1016/j.scitotenv.2010.06.056

Schroeder, W. H., & Munthe, J. (1998). Atmospheric mercury—An overview. *Atmospheric Environment*, *32*(5), 809–822. https://doi.org/10.1016/S1352-2310(97)00293-8

Schuster, P. F., Krabbenhoft, D. P., Naftz, D. L., Cecil, L. D., Olson, M. L., Dewild, J. F., et al. (2002). Atmospheric mercury deposition during the last 270 years: A glacial ice core record of natural and anthropogenic sources. *Environmental Science & Technology*, *36*(11), 2303–2310. https://doi.org/10.1021/es0157503

Schuster, P. F., Schaefer, K. M., Aiken, G. R., Antweiler, R. C., Dewild, J. F., Gryziec, J. D., et al. (2018). Permafrost stores a globally significant amount of mercury. *Geophysical Research Letters*, *45*, 1463–1471. https://doi.org/10.1002/2017GL075571

Schuster, P. F., Striegl, R. G., Aiken, G. R., Krabbenhoft, D. P., Dewild, J. F., Butler, K., et al. (2011). Mercury export from the Yukon river basin and potential response to a changing climate. *Environmental Science & Technology*, *45*(21), 9262–9267. https://doi.org/10.1021/es202068b

Schuur, E. A. G., Abbott, B., & Permafrost Carbon, N. (2011). High risk of permafrost thaw. *Nature*, *480*(7375), 32–33. https://doi.org/10.1038/480032a

Schwesig, D., Ilgen, G., & Matzner, E. (1999). Mercury and methylmercury in upland and wetland acid forest soils of a watershed in NE-Bavaria, Germany. *Water, Air, and Soil Pollution*, *113*(1/4), 141–154. https://doi.org/10.1023/A:1005080922234

Schwesig, D., & Matzner, E. (2001). Dynamics of mercury and methylmercury in forest floor and runoff of a forested watershed in Central Europe. *Biogeochemistry*, *53*(2), 181–200. https://doi.org/10.1023/A:1010600600099

Selvendiran, P., Driscoll, C. T., Bushey, J. T., & Montesdeoca, M. R. (2008). Wetland influence on mercury fate and transport in a temperate forested watershed. *Environmental Pollution*, *154*(1), 46–55. https://doi.org/10.1016/j.envpol.2007.12.005

Shaver, G. R., & Chapin, F. S. (1991). Production-biomass relationships and element cycling in contrasting Arctic vegetation types. *Ecological Monographs*, *61*(1), 1–31. https://doi.org/10.2307/1942997

Smith, D. B., & Geological Survey (U.S.) (2013). Geochemical and mineralogical data for soils of the conterminous United States. Reston, VA: U.S. Department of the Interior, U.S. Geological Survey.

Smith-Downey, N. V., Sunderland, E. M., & Jacob, D. J. (2010). Anthropogenic impacts on global storage and emissions of mercury from terrestrial soils: Insights from a new global model. *Journal of Geophysical Research*, *115*, G03008. https://doi.org/10.1029/2009JG001124

Soerensen, A. L., Jacob, D. J., Schartup, A. T., Fisher, J. A., Lehnherr, I., St, V. L., et al. (2016). A mass budget for mercury and methylmercury in the Arctic Ocean. *Global Biogeochemical Cycles*, *30*, 560–575. https://doi.org/10.1002/2015GB005280

StataCorp (2011). *Stata statistical software: Release 12*. College Station, TX: StataCorp LP.

Steffen, A., Douglas, T., Amyot, M., Ariya, P., Aspmo, K., Berg, T., et al. (2008). A synthesis of atmospheric mercury depletion event chemistry in the atmosphere and snow. *Atmospheric Chemistry and Physics*, *8*(6), 1445–1482. https://doi.org/10.5194/acp-8-1445-2008

Swain, E. B., Engstrom, D. R., Brigham, M. E., Henning, T. A., & Brezonik, P. L. (1992). Increasing rates of atmospheric mercury deposition in midcontinental North America. *Science*, *257*(5071), 784–787. https://doi.org/10.1126/science.257.5071.784

Tian, W., Egeland, G. M., Sobol, I., & Chan, H. M. (2011). Mercury hair concentrations and dietary exposure among Inuit preschool children in Nunavut, Canada. *Environment International*, *37*(1), 42–48. https://doi.org/10.1016/j.envint.2010.05.017

Turetsky, M. R., Kane, E. S., Harden, J. W., Ottmar, R. D., Manies, K. L., Hoy, E., & Kasischke, E. S. (2011). Recent acceleration of biomass burning and carbon losses in Alaskan forests and peatlands. *Nature Geoscience*, *4*(1), 27–31. https://doi.org/10.1038/ngeo1027

Turetsky, M. R., Harden, J. W., Friedli, H. R., Flannigan, M., Payne, N., Crock, J., & Radke, L. (2006). Wildfires threaten mercury stocks in northern soils. *Geophysical Research Letters*, *33*, L16403. https://doi.org/10.1029/2005GL025595

U.S. EPA (1999). Method IO 3.3, Compendium of Methods for the Determination of Inorganic Compounds in Ambient Air. Washington, DC.
Vörösmarty, C. J., Fekete, B. M., Meybeck, M., & Lammers, R. B. (2000). Global system of rivers: Its role in organizing continental land mass and defining land-to-ocean linkages. *Global Biogeochemical Cycles*, *14*(2), 599–621.
Wang, X., Luo, J., Yin, R., Yuan, W., Lin, C.-J., Sommar, J., et al. (2017). Using mercury isotopes to understand mercury accumulation in the montane forest floor of the eastern Tibetan Plateau. *Environmental Science & Technology*, *51*(2), 801–809. https://doi.org/10.1021/acs.est.6b03806
Webb, E. E., Schuur, E. A. G., Natali, S. M., Oken, K. L., Bracho, R., Krapek, J. P., et al. (2016). Increased wintertime CO_2 loss as a result of sustained tundra warming. *Biogeosciences*, *121*(2), 249–265.
Western Regional Climate Center, (2005). "Noatak, Alaska," accessed: 10/28/2016, http://www.raws.dri.edu/cgi-bin/rawMAIN.pl?akANOA.
Yang, Y., Yanai, R. D., Montesdeoca, M., & Driscoll, C. T. (2017). Measuring mercury in wood: challenging but important. *International Journal of Environmental Analytical Chemistry*, *97*, 456–467.
Yu, X., Driscoll, C. T., Warby, R. A. F., Montesdeoca, M., & Johnson, C. E. (2014). Soil mercury and its response to atmospheric mercury deposition across the northeastern United States. *Ecological Applications*, *24*(4), 812–822. https://doi.org/10.1890/13-0212.1
Zhang, T., Osterkamp, T. E., & Stamnes, K. (1996). Some characteristics of the climate in northern Alaska, USA. *Arctic and Alpine Research*, *28*(4), 509–518. https://doi.org/10.2307/1551862
Zhang, Y., Jacob, D. J., Dutkiewicz, S., Amos, H. M., Long, M. S., & Sunderland, E. M. (2015). Biogeochemical drivers of the fate of riverine mercury discharged to the global and Arctic oceans. *Global Biogeochemical Cycles*, *29*, 854–864. https://doi.org/10.1002/2015GB005124
Zheng, W., Obrist, D., Weis, D., & Bergquist, B. A. (2016). Mercury isotope compositions across North American forests. *Global Biogeochemical Cycles*, *30*, 1475–1492. https://doi.org/10.1002/2015GB005323